

Alpha kinase 3 signaling at the M-band maintains sarcomere integrity and proteostasis in striated muscle.

James W. McNamara^{1,2,3,4}, Benjamin L. Parker^{3,4}, Holly K. Voges^{1,2,5}, Neda R. Mehdiabadi¹, Francesca Bolk^{1,2,3}, Jin D. Chung^{1,3,4}, Natalie Charitakis¹, Jeffrey Molendijk³, Sean Lal⁶, Mirana Ramialison^{1,5,7,11}, Kathy Karavendzas¹, Hayley L. Pointer¹, Petros Syrris^{8,9}, Luis R. Lopes^{8,9}, Perry M. Elliott^{8,9}, Gordon S. Lynch^{3,4}, Richard J. Mills^{1,10}, James E. Hudson¹⁰, Kevin I. Watt^{1,11}, Enzo R. Porrello^{1,2,3,4,11*}, David A Elliott^{1,2,5,7,11*}.

1. Murdoch Children's Research Institute, The Royal Children's Hospital, Melbourne, Victoria, Australia.
2. Melbourne Centre for Cardiovascular Genomics and Regenerative Medicine, The Royal Children's Hospital, Melbourne, Victoria, Australia.
3. Department of Anatomy and Physiology, University of Melbourne, Victoria, Australia.
4. Centre for Muscle Research, University of Melbourne, Victoria, Australia.
5. School of Biomedical Sciences, and Department of Paediatrics, University of Melbourne, Victoria, Australia.
6. Precision Cardiovascular Laboratory, The University of Sydney, Sydney, New South Wales, Australia
7. Australian Regenerative Medicine Institute, Monash University, Wellington Road, Clayton, Victoria, Australia
8. Centre for Heart Muscle Disease, Institute of Cardiovascular Science, University College London, London, United Kingdom
9. Barts Heart Centre, St. Bartholomew's Hospital, Barts Health NHS Trust, London, United Kingdom
10. QIMR Berghofer Medical Research Institute, Brisbane 4006, QLD, Australia
11. The Novo Nordisk Foundation Centre for Stem Cell Medicine (reNEW), Murdoch Children's Research Institute, Victoria, Australia.

*Equal contribution.

Corresponding Authors: Enzo R. Porrello (enzo.porrello@mcri.edu.au), David A. Elliott (David.elliott@mcri.edu.au)

1 **SUMMARY**

2 Pathogenic variants in *alpha kinase 3 (ALPK3)* cause cardiomyopathy and musculoskeletal
3 disease. How *ALPK3* mutations result in disease remains unclear because little is known
4 about this atypical kinase. Using a suite of engineered human pluripotent stem cells (hPSCs)
5 we show that *ALPK3* localizes to the M-Band of the sarcomere. *ALPK3* deficiency disrupted
6 sarcomeric organization and calcium kinetics in hPSC-derived cardiomyocytes and reduced
7 force generation in cardiac organoids. Phosphoproteomic profiling identified *ALPK3*-
8 dependant phospho-peptides that were enriched for sarcomeric components of the M-band
9 and the ubiquitin-binding protein SQSTM1. Analysis of the *ALPK3* interactome confirmed
10 binding to M-band proteins including SQSTM1. Importantly, in hPSC-derived
11 cardiomyocytes modeling *ALPK3* deficiency and cardiomyopathic *ALPK3* mutations,
12 sarcomeric organization and M-band localization of SQSTM1 were abnormal. These data
13 suggest *ALPK3* has an integral role in maintaining sarcomere integrity and proteostasis in
14 striated muscle. We propose this mechanism may underly disease pathogenesis in patients
15 with *ALPK3* variants.

16

17

18

19

20 **Keywords**

21 Cardiomyopathy; Signaling; Cardiac Disease Modeling; Stem Cells

22

23

24

25

26 INTRODUCTION

27

28 Hypertrophic cardiomyopathy (HCM) is defined as the abnormal thickening of the left
29 ventricular wall, affecting an estimated 1 in 200 individuals (McNally et al., 2015; Semsarian
30 et al., 2015), making HCM the most common inherited cardiac disorder. Pathogenic variants
31 in genes encoding contractile proteins of the sarcomere are the most prevalent genetic
32 cause of HCM (Marian and Braunwald, 2017; Semsarian *et al.*, 2015). Critically, maintaining
33 sarcomere integrity relies on quality control mechanisms that identify and remove
34 components damaged under high mechanical and biochemical stress during muscle
35 contraction (Cohn et al., 2019; Martin and Kirk, 2020; Martin et al., 2021). The mechanisms
36 by which cardiomyocytes maintain sarcomere integrity are poorly understood. A key
37 mechanosensory mechanism linking the sarcomere to protein quality control pathways is
38 via the kinase domain of the giant sarcomeric protein titin which recruits the ubiquitin-binding
39 protein p62/sequestosome-1 (SQSTM1) to the M-band of the sarcomere (Lange et al., 2020;
40 Lange et al., 2005). Mutations in the titin kinase domain result in dislocation of SQSTM1
41 from the sarcomere into cytosolic aggregates. Very little is known about how sarcomeric
42 signaling cascades at the M-band coordinate protein quality control pathways to maintain
43 sarcomere integrity in striated muscle cells. Although coordinated phosphorylation of
44 sarcomeric proteins has long been recognized as integral to cardiac contractility (Solaro,
45 2008), few M-band kinases have been identified but include muscle creatine kinase,
46 phosphofructokinase, and the titin kinase domain (Hu et al., 2015; Lange et al., 2002; Lange
47 *et al.*, 2020; Wallimann et al., 1983). Therefore, defining the sarcomeric kinome and mode
48 of action of kinases is important to provide insights into muscle function and
49 cardiomyopathies.

50

51 Multiple genetic studies have linked variants in *alpha kinase 3* (ALPK3) with HCM (Almomani
52 et al., 2016; Aung et al., 2019; Herkert et al., 2020; Lopes et al., 2021; Phelan et al., 2016).
53 Furthermore, iPSC-derived cardiomyocytes from patients homozygous for *ALPK3* loss-of-
54 function variants recapitulate aspects of the HCM phenotype (Phelan *et al.*, 2016) and
55 *ALPK3* knockout mice develop cardiomyopathy (Van Sligtenhorst et al., 2012). ALPK3 is a
56 member of the atypical alpha kinase family which have low homology to conventional
57 kinases and are defined by the ability to phosphorylate residues within alpha helices
58 (Middelbeek et al., 2010). In immortalized cell lines, exogenously delivered ALPK3 appears
59 to localize to the nucleus (Hosoda et al., 2001) and thus it has been proposed to regulate
60 transcription factors (Almomani *et al.*, 2016). However, the kinase domain of ALPK3 is highly
61 similar to myosin heavy chain kinase (MHCK) which phosphorylates the tail of myosin heavy
62 chain in *Dictyostelium* to regulate cytoskeletal dynamics (Kuczmarski and Spudich, 1980).
63 Given the homology to MHCK, we hypothesized ALPK3 may play a similar role in
64 cytoskeletal signaling in the heart. Clinical data, cellular and animal models all demonstrate
65 that ALPK3 signaling is critical for cardiac function, therefore identifying the network of
66 cardiac proteins that rely on ALPK3 activity may provide insights into the intracellular
67 signaling mechanisms used to control cardiac contractility and, in turn, HCM disease
68 progression, while suggesting new therapeutic targets.

69
70 In this study, we addressed the hypothesis that ALPK3 acts as a cytoskeletal kinase, utilizing
71 *ALPK3* reporter and mutant hPSC lines, and mass spectrometry to define the role of ALPK3
72 in muscle contraction and signaling. Our data demonstrate that ALPK3 localizes to the M-
73 band of the sarcomere, which is a key regulatory node of sarcomere function (Lange *et al.*,
74 2020). We demonstrate that ALPK3 is required to maintain a functional contractile
75 apparatus. Furthermore, phosphoproteomic analysis revealed ALPK3 is required to

76 maintain phosphorylation of key sarcomeric proteins. Co-immunoprecipitation experiments
77 show that ALPK3 binds to known M-band components such as Obscurin (OBSCN). Finally,
78 ALPK3 physically binds to and is required for the sarcomeric localization of SQSTM1, an
79 important transporter of polyubiquitinated proteins (Liu et al., 2016; Pankiv et al., 2007).
80 These findings suggest that ALPK3 is an important component of the signaling network that
81 maintains functional sarcomeres.

82

83 RESULTS

84 **ALPK3 is a myogenic kinase localized to the M-band of the sarcomere.**

85 To define the expression of *ALPK3* in the human heart, we interrogated a single nucleus
86 RNA sequencing (snRNAseq) data set (Sim et al., 2021) of non-failing adult left ventricle
87 tissue (Figure 1A). *ALPK3* transcripts were enriched within cardiomyocytes (fold-enrichment
88 ~2.43, p-adj < 10^{-100}), but also to a lesser extent in smooth muscle cells (fold-enrichment
89 ~1.21, p-adj = 6.63E-05) (Figure 1B and Supplementary figure 1). To determine the sub-
90 cellular localization of *ALPK3*, we generated a series of *ALPK3*-reporter human pluripotent
91 stem cell (hPSC) lines in which either the tdTomato fluorescent protein or a Streptavidin-
92 Binding Peptide (SBP)-3xFLAG Tag (SBP-3xFLAG) were fused to the carboxyl-terminus of
93 *ALPK3* (Supplementary figure 2A-C). *ALPK3*-tdTomato was strongly expressed in alpha-
94 actinin expressing hPSC-derived cardiomyocytes (hPSC-CMs) but absent in CD90
95 expressing stromal cells (Figure 1C, Supplementary figure 2F). Critically, the *ALPK3*-
96 tdTomato fusion protein localized to the M-band of the sarcomere (Figure 1D and
97 Supplementary movie 1) as demonstrated by co-localization with the canonical M-band
98 protein Obscurin (OBSCN). Moreover, cellular fractionation studies, utilizing cardiomyocytes
99 derived from the *ALPK3*-SBP3xFLAG (Supplementary Figure 2 B-E) line revealed that
100 *ALPK3* associated with the myofilament protein fraction (Figure 1E). The clinical phenotype
101 of *ALPK3* mutations also includes musculoskeletal defects (Almomani *et al.*, 2016; Herkert
102 *et al.*, 2020; Phelan *et al.*, 2016). Using a publicly available snRNAseq data set for mouse
103 skeletal muscle, we found that *ALPK3* expression in skeletal muscle (McKellar et al., 2021)
104 is also restricted largely to myofibers (Supplementary figure 2G). In iPSC-derived skeletal
105 muscle cultures, *ALPK3*-tdTomato localized to the M-band, demonstrated by its localization
106 between z-disk marker alpha-actinin (Supplementary figure 2H). Together, these results
107 demonstrate that *ALPK3* is restricted to myocytes and is likely to function at the sarcomeric

108 M-band in striated muscle. Our finding that ALPK3 is found at the contractile apparatus of
109 myocytes challenges the current dogma that ALPK3 is a nuclear localized regulator of
110 transcription factors (Almomani *et al.*, 2016; Hosoda *et al.*, 2001). These data suggest an
111 alternative hypothesis that ALPK3 is a regulatory kinase controlling cardiac contraction via
112 phosphorylation of sarcomeric proteins.

113

114 **ALPK3 is required for sarcomere organization and calcium handling.**

115 To assess the regulatory role of ALPK3 in cardiomyocyte function, we utilized an *ALPK3*
116 loss-of-function mutant (*ALPK3^{c.1-60_+50del110}*, hereafter *ALPK3^{mut}*) hPSC cell line (Figure 2A,
117 Supplementary figure 3A-C) (Phelan *et al.*, 2016). Cardiac differentiation was unaffected in
118 *ALPK3^{mut}*, which produced a similar proportion of hPSC-derived cardiomyocytes (hPSC-
119 CMs) to wildtype cells, indicated by cardiac troponin-T (cTNT) expressing cells
120 (Supplementary Figure 3D). These findings suggest that, unlike its paralog ALPK2
121 (Hofsteen *et al.*, 2018), ALPK3 is not required for cardiogenesis. *ALPK3^{mut}* cardiomyocytes
122 displayed extensive sarcomeric disorganization and loss of the M-Band protein myomesin
123 (MYOM1), as well as the presence of stress fiber-like structures and alpha actinin containing
124 aggregates (Figure 2B). Calcium transients in single cardiomyocytes (Figure 2C and D)
125 recapitulated patient arrhythmogenicity in *ALPK3^{mut}* hPSC-CMs (Almomani *et al.*, 2016;
126 Phelan *et al.*, 2016) (Figure 2E). Peak cytosolic calcium levels (Figure 2F) were elevated
127 while calcium reuptake was delayed in *ALPK3^{mut}* myocytes (Figure 2G). These results
128 demonstrate that *ALPK3^{mut}* hPSC-CMs recapitulate key hallmarks of human *ALPK3* induced
129 cardiomyopathy and suggest ALPK3 plays a key role in maintaining sarcomere integrity.

130

131 **ALPK3 deficiency impairs contractility in cardiac organoids**

132 Human cardiac organoids (hCO) were generated (Mills et al., 2017) to assess changes in
133 contractile function between WT and *ALPK3^{mut}* heart cells (Figures 3A and B). Systolic force
134 generation was significantly reduced in *ALPK3^{mut}* hCOs (Figure 3C) together with a
135 reduction in beating rate (Figure 3D). Although no changes in contraction or relaxation
136 kinetics were observed (Figures 3E and F), *ALPK3^{mut}* hCOs were arrhythmogenic (Figure
137 3G). Immunofluorescent staining of hCOs with Z-disk marker ACTN2 and M-band marker
138 OBSCN revealed that sarcomeric organization, particularly at the M-band, was disrupted in
139 *ALPK3^{mut}* hCOs (Figure 3H). In addition, as observed in two-dimensional myocytes, some
140 aggregation of the M-band component OBSCN and the Z-disk component ACTN2 was
141 apparent in *ALPK3^{mut}* hCOs (Figure 3H). Collectively these results highlight the requirement
142 of ALPK3 to maintain force generation, sarcomere integrity and beating rhythmicity in three-
143 dimensional human cardiac tissue.

144

145 **ALPK3 deficient cardiomyocytes have compromised expression of key cardiac**
146 **protein networks.**

147 To define the ALPK3 dependent molecular networks we compared proteomic profiles of
148 purified wildtype and *ALPK3^{mut}* hPSC-CMs (Figure 4A) at days 14 (early) and 30 (late) of
149 cardiac differentiation (Supplementary Figure 4). Principal component analysis
150 demonstrated good reproducibility between replicates, with maturation-dependent changes
151 in the proteomic signature of *ALPK3^{mut}* cardiomyocytes (Supplementary Figure 4A). We
152 investigated altered biological processes at day 14 (2,335 differentially expressed proteins;
153 Figure 4B) and day 30 (2106 differentially expressed proteins; Figure 4D). At both
154 timepoints, pathways related to muscle structure, contraction, and stretch-sensing were
155 down regulated in *ALPK3^{mut}* cardiomyocytes (Figures 4C, E). Furthermore, *ALPK3^{mut}* hPSC-
156 CMs exhibited deregulation of pathways related to protein quality control (autophagy, protein

157 ubiquitination, sumoylation) and metabolism (glycolysis, fatty acid oxidation, creatine, and
158 ribonucleotide metabolism). Integration of early and late timepoints revealed divergence of
159 numerous differentially expressed proteins (Figure 4F), demonstrating the maturation- or
160 phenotype-dependent shifts in *ALPK3^{mut}* myocytes. Out of the 335 proteins commonly up-
161 or down-regulated at both timepoints (Figure 4F), pathways which regulate heart
162 development and contraction, sarcomere organization, and stretch detection were reduced
163 in *ALPK3^{mut}* cardiomyocytes (Figure 4G), while cell growth, metabolism, gene expression,
164 and microtubule polymerization pathways were enriched (Figure 4G). These data
165 collectively suggest that ALPK3 contributes to M-band signaling. Importantly, the M-Band is
166 understood to be a mechanosensitive regulator of sarcomere organization (Musa et al.,
167 2006), muscle metabolism (Hornemann et al., 2003), and protein turnover (Lange et al.,
168 2005).

169

170 Further, RNA-seq analysis revealed that transcriptional differences between WT and
171 *ALPK3^{mut}* hPSC-CMs were less pronounced at day 14 than day 30, suggesting the
172 transcriptional remodeling is secondary to dysregulation of the ALPK3-dependent proteome
173 (Supplementary Figure 5B). RNA-seq data, at both days 14 and 30, identified a suite of
174 commonly down-regulated genes in *ALPK3^{mut}* hPSC-CMs that were enriched in biological
175 processes related to heart development, contraction, and sarcomeric organization
176 (Supplementary figure 5C-F). The broad reduction in contractile protein levels was evident
177 albeit to a lesser extent in RNAseq data (Supplementary figure 6). These data suggest post-
178 transcriptional processes predominantly drive the phenotypic responses in *ALPK3* mutant
179 myocytes.

180

181 **ALPK3 is critical for phosphorylation of sarcomeric proteins and protein quality**
182 **control pathways.**

183 To understand potential ALPK3 dependent signaling pathways, we compared the global
184 phosphoproteomic profile of purified WT and *ALPK3^{mut}* cardiomyocytes, again at two points
185 of differentiation (Figure 5A). We detected 4,211 phosphorylated peptides with 1,671 and
186 806 peptides, normalized to total protein abundance, differentially phosphorylated at days
187 14 and 30, respectively (Figures 5B and D). At day 14, 1,659 peptides from 526 unique
188 proteins were dephosphorylated in *ALPK3^{mut}* myocytes, which associated with loss of
189 pathways related to sarcomere assembly, muscle contractility, and cell adhesion (Figure
190 5C). Autophagy components were dysregulated, suggesting this may either be a
191 generalized stress response (Singh et al., 2017) or that ALPK3 signaling may contribute to
192 the regulation of protein quality control in cardiomyocytes. Only 12 phosphopeptides from
193 12 unique proteins were increased in *ALPK3^{mut}* at day 14 (Figure 5B). Although the number
194 of dephosphorylated peptides was lower at day 30 (1,659 vs 307) the set of 154 unique
195 proteins identified was also enriched in GO terms related to cytoskeletal organization, heart
196 contraction, and cell adhesion (Figure 5E). At the day 30 timepoint (Figure 5D), the number
197 of enriched phosphopeptides observed in *ALPK3^{mut}* was dramatically higher than day 14
198 (499 vs. 12; the 499 peptides represent 271 unique proteins) suggesting increased
199 phosphorylation is a compensatory signaling response to extended stress with enriched
200 processes including stress response, glycolysis, RNA metabolism, and endosome transport.

201
202 There were 103 peptides from 58 unique proteins which were significantly dephosphorylated
203 in *ALPK3^{mut}* hPSC-CMs at both early and late timepoints (Figure 5F). In agreement with the
204 *ALPK3* cardiomyopathy phenotype (Almomani et al., 2016; Phelan et al., 2016) and
205 impaired contractility (Figure 2, 3), commonly dephosphorylated proteins were enriched in

206 regulation of cardiac contraction and cytoskeletal organization pathways (Figure 5G). Taken
207 together, these data reveal that ALPK3 contributes, either directly or indirectly, to the
208 phospho-regulation of key cytoskeletal proteins to maintain sarcomere organization and
209 function.

210

211 **ALPK3 binds SQSTM1 (p62) and is required for the sarcomeric localization of**
212 **SQSTM1.**

213 Our phosphoproteomic analyses indicated that ALPK3 deficiency caused
214 dephosphorylation of numerous proteins associated with sarcomere organization and
215 function as well as protein quality control. Cardiomyopathy, however, is itself linked to
216 remodeling of the phosphoproteome (Kuzmanov et al., 2016). Thus, this dataset alone is
217 not predictive of ALPK3 substrates. To address this, we performed mass spectrometry on
218 proteins enriched by co-immunoprecipitation (Co-IP) with endogenous ALPK3 carrying a 3
219 tandem repeat FLAG tag (Figure 6A and Supplementary Figure 2E). Together with ALPK3,
220 25 proteins were enriched with FLAG tagged ALPK3 hPSC-CMs over controls (Figure 6B).
221 Consistent with ALPK3's intracellular localization (Figure 1D, E) several known M-Band
222 proteins associated with ALPK3, such as obscurin (OBSCN) and obscurin-like protein
223 (OBSL1), demonstrating the fidelity of this Co-IP experiment. In addition to the sarcomeric
224 proteins, ALPK3 was found to interact with both the E3 ligase MURF2 (TRIM55) and the
225 ubiquitin-binding protein SQSTM1 (p62). Importantly, several ALPK3-bound proteins related
226 also demonstrated reduced phosphopeptide abundance (Supplementary figure 8). and
227 have been associated muscle pathology including OBSCN (Wu et al., 2021), OBSL1
228 (Blondelle et al., 2019), SQSTM1 (Bucelli et al., 2015), and HUWE1 (Dadson et al., 2017)
229 Both MURF2 and SQSTM1 are known to interact with titin kinase at the M-Band to regulate
230 mechanosensitive signaling and protein turnover (Lange *et al.*, 2005), we further

231 investigated the ALPK3-SQSTM1 interaction. We first validated the interaction using a
232 heterologous, non-muscle, system which confirmed the interaction between ALPK3 and
233 SQSTM1 when overexpressed in HEK293 cells (Figure 6C). Furthermore, ALPK3 and
234 SQSTM1 co-localized at the M-Band of hPSC-CMs (Figure 6D). While total SQSTM1 levels
235 were unchanged between wildtype and *ALPK3^{mut}* cultures (Figure 6E), SQSTM1 dislocated
236 from the sarcomere and became localized to cytosolic aggregates in *ALPK3^{mut}* hPSC-
237 derived cardiac and skeletal muscle cells (Figure 6F, Supplementary Figure 7). To
238 determine if M-band organization and SQSTM1 localization may underlie pathogenesis in
239 *ALPK3*-associated HCM, we generated three additional hPSC lines harboring *ALPK3*
240 variants (L639fs/34, Q1460X, R1792X) from a recently published cohort of patients with
241 HCM (Lopes *et al.*, 2021). Upon differentiation into cardiomyocytes, each of these *ALPK3*
242 patient variants recapitulated the key pathological features of sarcomere disorganization
243 and loss of M-Band myomesin (Figure 6G). Furthermore, SQSTM1 was not detected within
244 the sarcomeres of these patient variant hPSC lines but formed aggregates either within the
245 cytosol or at the cell membrane (Figure 6H). Collectively, these data suggest the binding of
246 ALPK3 to SQSTM1 is required for M-Band localization of SQSTM1 in striated muscle and
247 the disruption of the intracellular localization of SQSTM1 may be a prominent mechanism
248 driving ALPK3-related HCM. Thus, ALPK3 is integral to M-band integrity and signaling as
249 illustrated by the reduction of MYOM1 (Figure 2B and 6G), OBSCN (Figure 3H) and
250 SQSTM1 (Figure 6F, G) in ALPK3-deficient myocytes.

251

252

253

254 **DISCUSSION**

255 Our data show that ALPK3 is a myogenic kinase that localizes to the M-Band of sarcomeres
256 in striated muscle. We define the ALPK3-dependent phospho-proteome in hPSC-derived
257 cardiomyocytes at two stages of differentiation. Amongst the proteins that require ALPK3
258 for phosphorylation are components of the sarcomere, the functional unit that generates the
259 force underpinning muscle contraction. In addition, the phosphorylation status of the cellular
260 protein quality control system is also disrupted in ALPK3 mutant cardiomyocytes. In this
261 context, we identify that SQSTM1 and MURF2 both interact with ALPK3 and may provide a
262 mechanism whereby the M-band plays a key role in detecting and removing damaged
263 proteins from the sarcomere. Furthermore, ALPK3 is necessary for the M-band localization
264 of SQSTM1. In conclusion, these findings support a major role for ALPK3 in striated muscle
265 contraction and the intracellular signaling network regulating cardiomyocyte contractility.

266
267 Altered cardiomyocyte mechanotransduction is a common feature of cardiomyopathy (Lyon
268 et al., 2015), and while this has been extensively investigated in the context of Z-disk
269 signaling pathways (Buyandelger et al., 2011; Knöll et al., 2002; Martin *et al.*, 2021; Purcell
270 et al., 2004), comparatively little is understood about the contribution of M-Band biology. Our
271 findings suggest that ALPK3 is a component of the sarcomeric M-Band. Furthermore,
272 ALPK3 is critical for M-band integrity as the established M-Band marker MYOM1 was not
273 detected at the sarcomere of ALPK3 mutant cardiomyocytes. This loss of M-Band MYOM1
274 was also observed in cardiomyocytes harboring HCM-associated *ALPK3* variants. We
275 propose that ALPK3 forms a signaling node at the M-band that is required to maintain
276 sarcomere integrity (Figure 7). The titin kinase signalosome is the best understood pathway
277 at the M-Band. In this pathway, mechanical stretch induces a conformational change in the
278 kinase domain, which recruits protein quality control proteins NBR1, SQSTM1, and MURF2

279 to the M-Band (Lange *et al.*, 2005; Miller *et al.*, 2003; Perera *et al.*, 2011). This pathway
280 regulates cardiac proteostasis in response to mechanical stimuli via MURF2 regulation of
281 SRF gene expression and regulation of SQSTM1 localization (Lange *et al.*, 2020). Our data
282 indicates that ALPK3 may form a critical signaling network with titin kinase signaling, which
283 also binds SQSTM1 and MURF2 at the M-band, to link mechanical signals to protein quality
284 control networks. For example, the ALPK3-SQSTM1 interaction is required to maintain the
285 sarcomeric localization of SQSTM1, with ALPK3 deficiency leading to mis-localization of
286 SQSTM1 and impaired contractility in hPSC derived cardiomyocytes.

287
288 Given the longevity of human cardiac muscle cells, efficient protein quality control
289 mechanisms are essential to maintain cardiomyocyte function (Willis and Patterson, 2013).
290 The hypertrophic heart experiences sustained biomechanical and oxidative stress. Within
291 the myocyte, this translates to increased strain on contractile sarcomere proteins and higher
292 rates of protein misfolding (Henning and Brundel, 2017). While this misfolding is initially
293 compensated, protein quality control mechanisms cannot maintain the sustained activity
294 required for normal heart function. Indeed, aberrant protein quality control is a common
295 feature of HCM (Dorsch *et al.*, 2019; Gilda and Gomes, 2017; Henning and Brundel, 2017;
296 Singh *et al.*, 2017), which eventually leads to compromised cardiac structure and function.
297 In this context, the observation that ALPK3 interacts with protein homeostasis regulators
298 such as MURF2 and SQSTM1 within the M-Band suggests a role in controlling sarcomeric
299 proteostasis. This model of ALPK3 activity would be analogous to that seen for titin kinase
300 at the M-Band (Lange *et al.*, 2002; Lange *et al.*, 2020) and BAG3 at the Z-disc (Martin *et al.*,
301 2021) suggesting sarcomeric integrity is underpinned by the complex interplay of a number
302 for regulatory pathways. Given our results demonstrating mislocalization of SQSTM1 in
303 three independent ALPK3 pathogenic variants and the growing number of ALPK3 variants

304 linked to HCM(Herkert *et al.*, 2020; Lopes *et al.*, 2021), our findings point to a central role
305 for disrupted sarcomeric homeostasis in cardiomyopathy.

306

307 Our study demonstrates that ALPK3 is required to maintain sarcomere integrity and
308 contractile function in cardiomyocytes. Our findings define ALPK3 as a key functional
309 component of the M-Band in striated muscle. In addition, ALPK3 plays a role in regulating
310 protein quality control pathways via interactions with SQSTM1 and MURF2 at the M-band.
311 Given the dysregulation of protein quality control networks in cardiac disease, ALPK3 may
312 represent a promising therapeutic target to restore heart function in cardiomyopathies.

313

314

315 **Acknowledgements**

316 We acknowledge grant and fellowship support from the National Health and Medical
317 Research Council of Australia (E.R.P., D.A.E., B.L.P.), Australian Research Council
318 (E.R.P.), Heart Foundation of Australia (E.R.P., D.A.E), The Medical Research Future Fund
319 (E.R.P, D.A.E), The Stafford Fox Medical Research Foundation (E.R.P.), Australian
320 Genomics Health Alliance (J.W.M., E.R.P., and D.A.E.), the Royal Children's Hospital
321 Foundation (E.R.P.), and The MCRI Early Career Researcher Award (J.W.M.). MCRI is
322 supported by the Victorian Government's Operational Infrastructure Support Program.
323 E.R.P. and D.A.E. are Principal Investigators of The Novo Nordisk Foundation Center for
324 Stem Cell Medicine which is supported by a Novo Nordisk Foundation grant number
325 NNF21CC0073729. LRL is supported by an UKRI MRC clinical academic research
326 partnership (CARP) award (MR/T005181/1).

327

328 **Author Contributions**

329 J.W.M., E.R.P., and D.A.E. conceived the project. J.W.M., B.L.P., H.K.V., F.B., J.D.C.,
330 R.J.M., J.E.H., H.P., K.K., and P.S. performed experiments. J.W.M., B.L.P., H.K.V., N.R.M.,
331 N.C., J.M., M.R., and K.I.W. performed analyses. L.R.L, P.W.E, S.L., and G.S.L. contributed
332 key reagents. J.W.M., E.R.P. and D.A.E wrote the manuscript. All authors approved the final
333 version of the manuscript.

334

335 **Declarations of Interests**

336

337 R.J.M, J.E.H. and E.R.P. are co-founders, scientific advisors and hold equity in Dynamics,
338 a biotechnology company focused on the development of heart failure therapeutics.

339

340

341

342
343

344 REFERENCES

- 345
346 Almomani, R., Verhagen, J.M.A., Herkert, J.C., Brosens, E., van Spaendonck-Zwarts, K.Y.,
347 Asimaki, A., van der Zwaag, P.A., Frohn-Mulder, I.M.E., Bertoli-Avella, A.M., Boven, L.G.,
348 et al. (2016). Biallelic Truncating Mutations in ALPK3 Cause Severe Pediatric
349 Cardiomyopathy. *Journal of the American College of Cardiology* 67, 515-525.
350 <https://doi.org/10.1016/j.jacc.2015.10.093>.
- 351 Aung, N., Vargas, J.D., Yang, C., Cabrera, C.P., Warren, H.R., Fung, K., Tzanis, E., Barnes,
352 M.R., Rotter, J.I., Taylor, K.D., et al. (2019). Genome-Wide Analysis of Left Ventricular
353 Image-Derived Phenotypes Identifies Fourteen Loci Associated With Cardiac
354 Morphogenesis and Heart Failure Development. *Circulation* 140, 1318-1330.
355 [10.1161/circulationaha.119.041161](https://doi.org/10.1161/circulationaha.119.041161).
- 356 Blondelle, J., Marrocco, V., Clark, M., Desmond, P., Myers, S., Nguyen, J., Wright, M.,
357 Bremner, S., Pierantozzi, E., Ward, S., et al. (2019). Murine obscurin and Obsl1 have
358 functionally redundant roles in sarcolemmal integrity, sarcoplasmic reticulum organization,
359 and muscle metabolism. *Commun Biol* 2, 178. [10.1038/s42003-019-0405-7](https://doi.org/10.1038/s42003-019-0405-7).
- 360 Bucelli, R.C., Arhzaouy, K., Pestronk, A., Pittman, S.K., Rojas, L., Sue, C.M., Evilä, A.,
361 Hackman, P., Udd, B., Harms, M.B., and Weihl, C.C. (2015). SQSTM1 splice site mutation
362 in distal myopathy with rimmed vacuoles. *Neurology* 85, 665-674.
363 [10.1212/wnl.0000000000001864](https://doi.org/10.1212/wnl.0000000000001864).
- 364 Buyandelger, B., Ng, K.-E., Miocic, S., Piotrowska, I., Gunkel, S., Ku, C.-H., and Knöll, R.
365 (2011). MLP (muscle LIM protein) as a stress sensor in the heart. *Pflügers Archiv : European*
366 *journal of physiology* 462, 135-142. [10.1007/s00424-011-0961-2](https://doi.org/10.1007/s00424-011-0961-2).

- 367 Cohn, R., Thakar, K., Lowe, A., Ladha, F.A., Pettinato, A.M., Romano, R., Meredith, E.,
368 Chen, Y.S., Atamanuk, K., Huey, B.D., and Hinson, J.T. (2019). A Contraction Stress Model
369 of Hypertrophic Cardiomyopathy due to Sarcomere Mutations. *Stem Cell Reports* 12, 71-
370 83. [10.1016/j.stemcr.2018.11.015](https://doi.org/10.1016/j.stemcr.2018.11.015).
- 371 Dadson, K., Hauck, L., Hao, Z., Grothe, D., Rao, V., Mak, T.W., and Billia, F. (2017). The
372 E3 ligase Mule protects the heart against oxidative stress and mitochondrial dysfunction
373 through Myc-dependent inactivation of Pgc-1 α and Pink1. *Sci Rep* 7, 41490.
374 [10.1038/srep41490](https://doi.org/10.1038/srep41490).
- 375 Dorsch, L.M., Schuldt, M., dos Remedios, C.G., Schinkel, A.F.L., de Jong, P.L., Michels, M.,
376 Kuster, D.W.D., Brundel, B., and van der Velden, J. (2019). Protein Quality Control
377 Activation and Microtubule Remodeling in Hypertrophic Cardiomyopathy. *Cells* 8.
378 [10.3390/cells8070741](https://doi.org/10.3390/cells8070741).
- 379 Gilda, J.E., and Gomes, A.V. (2017). Proteasome dysfunction in cardiomyopathies. *Journal*
380 *of Physiology* 595, 4051-4071. [10.1113/jp273607](https://doi.org/10.1113/jp273607).
- 381 Henning, R.H., and Brundel, B.J.J.M. (2017). Proteostasis in cardiac health and disease.
382 *Nature Reviews Cardiology* 14, 637-653. [10.1038/nrcardio.2017.89](https://doi.org/10.1038/nrcardio.2017.89).
- 383 Herkert, J.C., Verhagen, J.M.A., Yotti, R., Haghghi, A., Phelan, D.G., James, P.A., Brown,
384 N.J., Stutterd, C., Macciocca, I., Leong, K., et al. (2020). Expanding the clinical and genetic
385 spectrum of ALPK3 variants: Phenotypes identified in pediatric cardiomyopathy patients and
386 adults with heterozygous variants. *American Heart Journal* 225, 108-119.
387 [10.1016/j.ahj.2020.03.023](https://doi.org/10.1016/j.ahj.2020.03.023).

- 388 Hofsteen, P., Robitaille, A.M., Strash, N., Palpant, N., Moon, R.T., Pabon, L., and Murry,
389 C.E. (2018). ALPK2 Promotes Cardiogenesis in Zebrafish and Human Pluripotent Stem
390 Cells. *iScience* 2, 88-100. 10.1016/j.isci.2018.03.010.
- 391 Hornemann, T., Kempa, S., Himmel, M., Hayess, K., Fürst, D.O., and Wallimann, T. (2003).
392 Muscle-type creatine kinase interacts with central domains of the M-band proteins
393 myomesin and M-protein. *Journal of Molecular Biology* 332, 877-887. 10.1016/s0022-
394 2836(03)00921-5.
- 395 Hosoda, T., Monzen, K., Hiroi, Y., Oka, T., Takimoto, E., Yazaki, Y., Nagai, R., and Komuro,
396 I. (2001). A novel myocyte-specific gene Midori promotes the differentiation of P19CL6 cells
397 into cardiomyocytes. *Journal of Biological Chemistry* 276, 35978-35989.
398 10.1074/jbc.M100485200.
- 399 Hu, L.-Y.R., Ackermann, M.A., and Kontrogianni-Konstantopoulos, A. (2015). The
400 Sarcomeric M-Region: A Molecular Command Center for Diverse Cellular Processes.
401 *BioMed Research International* 2015, 714197. 10.1155/2015/714197.
- 402 Knöll, R., Hoshijima, M., Hoffman, H.M., Person, V., Lorenzen-Schmidt, I., Bang, M.L.,
403 Hayashi, T., Shiga, N., Yasukawa, H., Schaper, W., et al. (2002). The cardiac mechanical
404 stretch sensor machinery involves a Z disc complex that is defective in a subset of human
405 dilated cardiomyopathy. *Cell* 111, 943-955. 10.1016/s0092-8674(02)01226-6.
- 406 Kuczarski, E.R., and Spudich, J.A. (1980). Regulation of myosin self-assembly:
407 phosphorylation of Dictyostelium heavy chain inhibits formation of thick filaments.
408 *Proceedings of the National Academy of Sciences* 77, 7292-7296.
409 10.1073/pnas.77.12.7292.

- 410 Kuzmanov, U., Guo, H., Buchsbaum, D., Cosme, J., Abbasi, C., Isserlin, R., Sharma, P.,
411 Gramolini, A.O., and Emili, A. (2016). Global phosphoproteomic profiling reveals perturbed
412 signaling in a mouse model of dilated cardiomyopathy. *Proceedings of the National
413 Academy of Sciences* *113*, 12592-12597. [10.1073/pnas.1606444113](https://doi.org/10.1073/pnas.1606444113).
- 414 Lange, S., Auerbach, D., McLoughlin, P., Perriard, E., Schäfer, B.W., Perriard, J.-C., and
415 Ehler, E. (2002). Subcellular targeting of metabolic enzymes to titin in heart muscle may be
416 mediated by DRAL/FHL-2. *Journal of Cell Science* *115*, 4925-4936. [10.1242/jcs.00181](https://doi.org/10.1242/jcs.00181).
- 417 Lange, S., Pinotsis, N., Agarkova, I., and Ehler, E. (2020). The M-band: The underestimated
418 part of the sarcomere. *Biochimica et Biophysica Acta (BBA) - Molecular Cell Research* *1867*,
419 118440. <https://doi.org/10.1016/j.bbamcr.2019.02.003>.
- 420 Lange, S., Xiang, F., Yakovenko, A., Vihola, A., Hackman, P., Rostkova, E., Kristensen, J.,
421 Brandmeier, B., Franzen, G., Hedberg, B., et al. (2005). The Kinase Domain of Titin Controls
422 Muscle Gene Expression and Protein Turnover. *Science* *308*, 1599-1603.
423 [doi:10.1126/science.11110463](https://doi.org/10.1126/science.11110463).
- 424 Liu, W.J., Ye, L., Huang, W.F., Guo, L.J., Xu, Z.G., Wu, H.L., Yang, C., and Liu, H.F. (2016).
425 p62 links the autophagy pathway and the ubiquitin–proteasome system upon ubiquitinated
426 protein degradation. *Cellular & Molecular Biology Letters* *21*, 29. [10.1186/s11658-016-0031-](https://doi.org/10.1186/s11658-016-0031-z)
427 [Z](https://doi.org/10.1186/s11658-016-0031-z).
- 428 Lopes, L.R., Garcia-Hernández, S., Lorenzini, M., Futema, M., Chumakova, O.,
429 Zateyshchikov, D., Isidoro-Garcia, M., Villacorta, E., Escobar-Lopez, L., Garcia-Pavia, P., et
430 al. (2021). Alpha-protein kinase 3 (ALPK3) truncating variants are a cause of autosomal
431 dominant hypertrophic cardiomyopathy. *European Heart Journal* *42*, 3063-3073.
432 [10.1093/eurheartj/ehab424](https://doi.org/10.1093/eurheartj/ehab424).

- 433 Lyon, R.C., Zanella, F., Omens, J.H., and Sheikh, F. (2015). Mechanotransduction in cardiac
434 hypertrophy and failure. *Circulation research* *116*, 1462-1476.
435 10.1161/CIRCRESAHA.116.304937.
- 436 Marian, A.J., and Braunwald, E. (2017). Hypertrophic cardiomyopathy: genetics,
437 pathogenesis, clinical manifestations, diagnosis, and therapy. *Circulation research* *121*,
438 749-770.
- 439 Martin, T.G., and Kirk, J.A. (2020). Under construction: The dynamic assembly,
440 maintenance, and degradation of the cardiac sarcomere. *Journal of Molecular and Cellular*
441 *Cardiology* *148*, 89-102. 10.1016/j.yjmcc.2020.08.018.
- 442 Martin, T.G., Myers, V.D., Dubey, P., Dubey, S., Perez, E., Moravec, C.S., Willis, M.S.,
443 Feldman, A.M., and Kirk, J.A. (2021). Cardiomyocyte contractile impairment in heart failure
444 results from reduced BAG3-mediated sarcomeric protein turnover. *Nature Communications*
445 *12*, 2942. 10.1038/s41467-021-23272-z.
- 446 McKellar, D.W., Walter, L.D., Song, L.T., Mantri, M., Wang, M.F.Z., De Vlaminck, I., and
447 Cosgrove, B.D. (2021). Large-scale integration of single-cell transcriptomic data captures
448 transitional progenitor states in mouse skeletal muscle regeneration. *Communications*
449 *Biology* *4*, 1280. 10.1038/s42003-021-02810-x.
- 450 McNally, E.M., Barefield, D.Y., and Puckelwartz, M.J. (2015). The genetic landscape of
451 cardiomyopathy and its role in heart failure. *Cell Metabolism* *21*, 174-182.
452 10.1016/j.cmet.2015.01.013.
- 453 Middelbeek, J., Clark, K., Venselaar, H., Huynen, M.A., and van Leeuwen, F.N. (2010). The
454 alpha-kinase family: an exceptional branch on the protein kinase tree. *Cell Mol Life Sci* *67*,
455 875-890. 10.1007/s00018-009-0215-z.

- 456 Miller, G., Musa, H., Gautel, M., and Peckham, M. (2003). A targeted deletion of the C-
457 terminal end of titin, including the titin kinase domain, impairs myofibrillogenesis. *Journal of*
458 *Cell Science* 116, 4811-4819. [10.1242/jcs.00768](https://doi.org/10.1242/jcs.00768).
- 459 Mills, R.J., Titmarsh, D.M., Koenig, X., Parker, B.L., Ryall, J.G., Quaife-Ryan, G.A., Voges,
460 H.K., Hodson, M.P., Ferguson, C., Drowley, L., et al. (2017). Functional screening in human
461 cardiac organoids reveals a metabolic mechanism for cardiomyocyte cell cycle arrest.
462 *Proceedings of the National Academy of Sciences* 114, E8372-E8381.
463 [10.1073/pnas.1707316114](https://doi.org/10.1073/pnas.1707316114).
- 464 Musa, H., Meek, S., Gautel, M., Peddie, D., Smith, A.J.H., and Peckham, M. (2006).
465 Targeted homozygous deletion of M-band titin in cardiomyocytes prevents sarcomere
466 formation. *Journal of Cell Science* 119, 4322-4331. [10.1242/jcs.03198](https://doi.org/10.1242/jcs.03198).
- 467 Pankiv, S., Clausen, T.H., Lamark, T., Brech, A., Bruun, J.A., Outzen, H., Øvervatn, A.,
468 Bjørkøy, G., and Johansen, T. (2007). p62/SQSTM1 binds directly to Atg8/LC3 to facilitate
469 degradation of ubiquitinated protein aggregates by autophagy. *Journal of Biological*
470 *Chemistry* 282, 24131-24145. [10.1074/jbc.M702824200](https://doi.org/10.1074/jbc.M702824200).
- 471 Perera, S., Holt, M.R., Mankoo, B.S., and Gautel, M. (2011). Developmental regulation of
472 MURF ubiquitin ligases and autophagy proteins nbr1, p62/SQSTM1 and LC3 during cardiac
473 myofibril assembly and turnover. *Developmental Biology* 351, 46-61.
474 <https://doi.org/10.1016/j.ydbio.2010.12.024>.
- 475 Phelan, D.G., Anderson, D.J., Howden, S.E., Wong, R.C., Hickey, P.F., Pope, K., Wilson,
476 G.R., Pébay, A., Davis, A.M., Petrou, S., et al. (2016). ALPK3-deficient cardiomyocytes
477 generated from patient-derived induced pluripotent stem cells and mutant human embryonic
478 stem cells display abnormal calcium handling and establish that ALPK3 deficiency underlies

- 479 familial cardiomyopathy. *European Heart Journal* 37, 2586-2590.
480 [10.1093/eurheartj/ehw160](https://doi.org/10.1093/eurheartj/ehw160).
- 481 Purcell, N.H., Darwis, D., Bueno, O.F., Müller, J.M., Schüle, R., and Molkenin, J.D. (2004).
482 Extracellular signal-regulated kinase 2 interacts with and is negatively regulated by the LIM-
483 only protein FHL2 in cardiomyocytes. *Molecular and Cellular Biology* 24, 1081-1095.
484 [10.1128/mcb.24.3.1081-1095.2004](https://doi.org/10.1128/mcb.24.3.1081-1095.2004).
- 485 Semsarian, C., Ingles, J., Maron, M.S., and Maron, B.J. (2015). New perspectives on the
486 prevalence of hypertrophic cardiomyopathy. *Journal of the American College of Cardiology*
487 65, 1249-1254. [10.1016/j.jacc.2015.01.019](https://doi.org/10.1016/j.jacc.2015.01.019).
- 488 Sim, C.B., Phipson, B., Ziemann, M., Rafehi, H., Mills, R.J., Watt, K.I., Abu-Bonsrah, K.D.,
489 Kalathur, R.K.R., Voges, H.K., Dinh, D.T., et al. (2021). Sex-Specific Control of Human Heart
490 Maturation by the Progesterone Receptor. *Circulation* 143, 1614-1628.
491 [10.1161/circulationaha.120.051921](https://doi.org/10.1161/circulationaha.120.051921).
- 492 Singh, S.R., Zech, A.T.L., Geertz, B., Reischmann-Düsener, S., Osinska, H., Prondzynski,
493 M., Krämer, E., Meng, Q., Redwood, C., van der Velden, J., et al. (2017). Activation of
494 Autophagy Ameliorates Cardiomyopathy in Mybpc3-Targeted Knockin Mice. *Circulation:*
495 *Heart Failure* 10. [10.1161/circheartfailure.117.004140](https://doi.org/10.1161/circheartfailure.117.004140).
- 496 Solaro, R.J. (2008). Multiplex Kinase Signaling Modifies Cardiac Function at the Level of
497 Sarcomeric Proteins. *Journal of Biological Chemistry* 283, 26829-26833.
498 <https://doi.org/10.1074/jbc.R800037200>.
- 499 Van Sligtenhorst, I., Ding, Z.M., Shi, Z.Z., Read, R.W., Hansen, G., and Vogel, P. (2012).
500 Cardiomyopathy in α -kinase 3 (ALPK3)-deficient mice. *Veterinary Pathology* 49, 131-141.
501 [10.1177/0300985811402841](https://doi.org/10.1177/0300985811402841).

502 Wallimann, T., Doetschman, T.C., and Eppenberger, H.M. (1983). Novel staining pattern of
503 skeletal muscle M-lines upon incubation with antibodies against MM-creatine kinase.
504 *Journal of Cell Biology* 96, 1772-1779. [10.1083/jcb.96.6.1772](https://doi.org/10.1083/jcb.96.6.1772).

505 Willis, M.S., and Patterson, C. (2013). Proteotoxicity and Cardiac Dysfunction — Alzheimer's
506 Disease of the Heart? *New England Journal of Medicine* 368, 455-464.
507 [10.1056/NEJMra1106180](https://doi.org/10.1056/NEJMra1106180).

508 Wu, G., Liu, J., Liu, M., Huang, Q., Ruan, J., Zhang, C., Wang, D., Sun, X., Jiang, W., Kang,
509 L., et al. (2021). Truncating Variants in OBSCN Gene Associated With Disease-Onset and
510 Outcomes of Hypertrophic Cardiomyopathy. *Circ Genom Precis Med* 14, e003401.
511 [10.1161/circgen.121.003401](https://doi.org/10.1161/circgen.121.003401).

512

513

514 **METHODS**

515 **Single Nuclei RNAseq Bioinformatic Analysis**

516 Raw fastq reads for each sample were mapped, processed, and counted using Cell Ranger (v3.0.2).
517 Following this, the counts were then aggregated together to create a table of unique molecular
518 identifier (UMI) counts for 33,939 genes for each of the samples. All pre-processing and filtering
519 steps of the datasets were subsequently carried out using the R statistical programming language
520 (v3.6.0). The quality of the nuclei was assessed for each sample independently by examining the
521 distributions of total UMI counts, the number of unique genes detected per sample and the
522 proportions of ribosomal and mitochondrial content per nuclei. In brief, after removing ambient RNA
523 contamination using SoupX(Young and Behjati, 2020), nuclei were removed from an experiment if:
524 1) the number of genes detected was less than predefined lower outlier cut-off, 2) the number of
525 UMI for the nuclei was less than a predefined lower outlier cut-off, 3) the percent of mitochondrial
526 gene content was greater than 5%, and 4) the percent of ribosomal gene content was greater than
527 5%. The lower outlier cut-off was calculated as the first quartile minus 1.5 times the interquartile
528 range. Subsequently, DoubletFinder(v2.0.3)(McGinnis et al., 2019) was used to remove potential
529 doublets into downstream clustering. It was followed by gene filtering in which mitochondrial and
530 ribosomal genes were discarded, as well as genes that were not annotated. Genes that had at least
531 1 count in at least 20 nuclei were retained for further analysis, assuming a minimum cluster size of
532 20 nuclei. All genes on the X and Y chromosomes were removed before clustering and all
533 subsequent analysis. After removing poor-quality nuclei, very low-expressed and non-informative
534 genes as well as genes on X and Y chromosome, for each sample, we performed SCTransform
535 normalization(Stuart et al., 2019), data integration of the three biological replicates(Butler et al.,
536 2018; Stuart *et al.*, 2019; Stuart and Satija, 2019), data scaling and graph-based clustering
537 separately, using the R package Seurat (v3.0.2). Data integration of the biological replicates for each
538 group was performed using CCA³ from the Seurat package with 30 dimensions and 3000 integration
539 anchors followed by data scaling. Clustering of the nuclei was performed with 20 principal
540 components (PCs) and an initial resolution of 0.3. Marker genes to annotate clusters were identified
541 as significantly up-regulated genes for each cluster using moderated t-tests, accounting for the mean

542 variance trend and employing robust empirical Bayes shrinkage of the variances, followed by TREAT
543 tests specifying a log-fold-change threshold of 0.5 and false discovery rate (FDR) cut off <0.05, using
544 the limma R package (v3.40.2).

545

546 **Stem Cell Culture and Cardiac Differentiation**

547 The female HES3 *NKX^{eGFP/+}* human embryonic stem cell line was used for all experiments, and has
548 previously been described (Elliott et al., 2011). The *ALPK3^{mut}* loss of function hPSC line was
549 generated previously using CRISPR/Cas9(Phelan et al., 2016). Stem cells were routinely passaged
550 using Tryple (ThermoFisher Scientific 12604013) onto GelTrex (ThermoFisher Scientific A1413301)
551 coated flasks and mTeSR plus medium (STEMCELL Technologies Catalog #05825). The selective
552 ROCK1 inhibitor Y-27632 (Selleckchem S6390) was used when passaging. Differentiation into
553 hPSC-CMs was performed using a monolayer culture system with small molecule wnt-
554 activation/inhibition protocol(Sim et al., 2021). Briefly, stem cells were plated on day -2 at 20,000
555 cells per cm² with mTeSR plus (with 10μM Y-27632). The next day, the medium was refreshed
556 (without Y-27632). On day 0 of the differentiation, the medium was switched to basal differentiation
557 medium (RPMI 1640 supplemented with 2% B-27 minus vitamin A, 1% GlutaMax, 1%
558 Penicillin/Streptomycin) plus 80ng/ml Activin A (R&D Systems 338-AC), 8mM CHIR99021 (Tocris
559 4423), and 50ug/ml ascorbic acid (Sigma Aldrich A5960). Twenty-four hours later, the media was
560 replaced with fresh basal differentiation medium. On day 3, the medium was exchanged to basal
561 differentiation medium containing 5mM IWR-1 (Sigma-Aldrich I0161) and 50ug/ml ascorbic acid. 72
562 hours later, cells were switched back to basal differentiation media and maintained with media
563 changes every 48 hours. To enrich for myocyte populations, cardiac differentiations were treated for
564 96 hours with glucose-free DMEM containing 5mM sodium L-lactate, 1% GlutaMax, and 1%
565 Penicillin/Streptomycin, with media exchange at 48 hours.

566

567 **Genome Editing**

568 Genome editing was performed using CRISPR/Cas9 (Clustered Regularly Interspaced Short
569 Palindromic Repeats/Cas9). To generate 3' tagged ALPK3 cell lines, the guide sequence 5'-

570 GCCCCCAGCCTCTGCGG-3' was cloned into the vector pSpCas9(BB)-2A-eGFP (PX458 plasmid
571 a gift from Feng Zhang, Addgene #48138). Homology directed repair templates were designed to
572 contain 1000bp homology arms flanking the region to be edited. HES3 *NKX^{eGFP/+}* human embryonic
573 stem cells were nucleofected with the PX458 and repair plasmids. Annealed oligonucleotides were
574 also cloned into the pSpCas9(BB)-2A-eGFP vector for guide RNA sequences in *ALPK3* patient
575 variant cell lines. Sequences for each guide RNA were as follows: *ALPK3^{L639fs/34}* 5'-
576 CCAGGCGCCCGGACACTCA-3' , *ALPK3^{Q1460X}* 5'-GGCCCTGGATGAAGGCAAGC-3', and
577 *ALPK3^{R1792X}* 5'-GATTGCTACCAAACCTCCGA-3'. Homology directed repair templates were ~80mer
578 ssODNs containing variants plus synonymous variants to prevent re-cutting by Cas9 of correctly
579 targeted DNA. HES3 *NKX^{eGFP/+}* human embryonic stem cells were co-transfected with ssODN and
580 PX458 using lipofectamine 3000 with the PX458. Single GFP-expressing cells were sorted into 96
581 well plates and screened by PCR.

582

583 **Flow Cytometry**

584 Cardiac differentiations were dissociated using 0.25% trypsin EDTA (Gibco #25200056) and filtered
585 to a single cell suspension. For intracellular flow, cells were fixed in 2% paraformaldehyde (PFA) for
586 10 minutes prior to permeabilization with 0.25% triton X-100. Primary antibody staining used alpha
587 actinin (Sigma-Aldrich A7811 (Abcam ab11370) as cardiomyocyte markers. Data was acquired on
588 an LSRFortessa X-20 Cell Analyzer.

589

590 **Immunofluorescence**

591 Cells were washed with PBS before fixation with 2% PFA for 30 minutes at room temperature. Prior
592 to staining, cells were permeabilised in 0.1% triton X-100 in PBS for 30 minutes and blocked in 5%
593 BSA in PBS-T for 1 hour. Primary antibodies were incubated overnight at 4°C. Cells were washed 3
594 times for 5 minutes in PBS-T before incubation with secondary antibodies for 1 hour at room
595 temperature.

596

597 **Sample Preparation for Global (Phospho)proteomics**

598 Samples were washed three times with ice cold PBS on ice. The cells were then scraped off the dish
599 using 4% (w/v) sodium deoxycholate in 100mM tris-HCl, pH 8.5 before heating at 95°C for 5 minutes.
600 Cell lysates were allowed to cool on ice for 5 minutes prior to snap freezing on dry ice and stored at
601 -80°C. Samples were thawed on ice, quantified with BCA assay (ThermoFisher Scientific) and
602 normalized to 300 µg / 200 µl. Protein was reduced with a final concentration of 10 mM Tris(2-
603 carboxyethyl)phosphine hydrochloride (TCEP) (Sigma) and alkylated with 40 mM 2-chloroacetamide
604 (CAA) (Sigma) for 5 min at 45°C. Samples were cooled on ice and then digested with 3 µg of
605 sequencing grade trypsin (Sigma) and 3 µg of sequencing grade LysC (Wako) overnight at 37°C. A
606 five µg aliquot was removed for total proteomic analysis and the phosphopeptides enriched from the
607 remaining digest using a the EasyPhos protocol as previously described(Humphrey et al., 2018).

608

609 **Sample Preparation for ALPK3 Interactome**

610 Protein G Dynabeads were resuspended in 50 µl of 2M urea, 50mM Tris pH 7.5 containing 1mM
611 TCEP, 5mM CAA and 0.2ug trypsin and 0.2ug of LysC and digested overnight at 37°C with shaking
612 at 1800RPM. Peptides were removed, diluted with 150 µl of 1% trifluoroacetic acid (TFA) and
613 desalted on poly(styrenedivinybenzene)-reversed phase support (SDB-RPS) micro-columns
614 (Sigma) as described previously(Humphrey *et al.*, 2018). The columns were washed with 99%
615 isopropanol containing 1% TFA followed by 5% acetonitrile containing 0.2% TFA and then eluted
616 with 80% acetonitrile containing 1% ammonium hydroxide and dried by vacuum centrifugation.

617

618 **LC-MS/MS Acquisition**

619 Peptides were resuspended in 2% acetonitrile containing 0.1% TFA and analysed on a Dionex 3500
620 nanoHPLC, coupled to an Orbitrap Eclipse mass spectrometer (ThermoFischer Scientific) via
621 electrospray ionization in positive mode with 1.9 kV at 275 °C and RF set to 40%. Separation was
622 achieved on a 50 cm × 75 µm column packed with C18AQ (1.9 µm; Dr Maisch, Ammerbuch,
623 Germany) (PepSep, Marslev, Denmark) over 60 min at a flow rate of 300 nL/min. The peptides were
624 eluted over a linear gradient of 3–40% Buffer B (Buffer A: 0.1% formic acid; Buffer B: 80% v/v
625 acetonitrile, 0.1% v/v FA) and the column was maintained at 50 °C. The instrument was operated in

626 data-independent acquisition mode with an MS1 spectrum acquired over the mass range 350–950
627 m/z (60,000 resolution, 2.5 x 10⁶ automatic gain control (AGC) and 50 ms maximum injection time)
628 followed by MS/MS analysis with HCD of 37 x 16 m/z with 1 m/z overlap (28% normalized collision
629 energy, 30,000 resolution, 1 x 10⁶ AGC, automatic injection time).

630

631 **LC-MS/MS Data Processing**

632 Data were searched against the UniProt human database (June 2021; UP000000589_109090 and
633 UP000000589_109090_additional) with Spectronaut 15.1.210713.50606 using default parameters
634 with peptide spectral matches, peptide and protein false discovery rate (FDR) set to 1%. All data
635 were searched with oxidation of methionine set as the variable modification and
636 carbamidomethylation set as the fixed modification. For analysis of phosphopeptides,
637 phosphorylation of Serine, Threonine and Tyrosine was set as a variable modification. Quantification
638 was performed using MS2-based extracted ion chromatograms employing 3-6 fragment ions
639 >450 m/z with automated fragment-ion interference removal as described previously (Bruderer et al.,
640 2015).

641

642 **Proteomic and Phosphoproteomic statistical and downstream analysis**

643 Data were processed with Perseus (Tyanova et al., 2016) to remove decoy data, potential
644 contaminants and proteins only identified with a single peptide containing oxidized methionine. The
645 “Expand Site” function was additionally used for phosphoproteomic data to account for multi-
646 phosphorylated peptides prior to statistical analysis. For analysis of phosphoproteomic and
647 proteomic data were Log₂-transformed and normalized by subtracting the median of each sample.
648 Data were filtered to contain phosphosites quantified in at least 3 biological replicates and statistical
649 analysis performed with ANOVA including correction for multiple hypothesis testing using Benjamini
650 Hochberg FDR with $q < 0.05$ defined as a significance cut-off. For analysis of interactome data were
651 Log₂-transformed and normalized by subtracting the median of each sample. Data were filtered to
652 contain proteins quantified in at least 3 biological replicates of the ALPK3 pull-down group. Data with
653 missing data in all the replicates of the negative control group were imputed using random values

654 from a down-shifted normalized distribution of the entire dataset. Differentially enriched proteins
655 were calculated using t-tests including correction for multiple hypothesis testing using Benjamini
656 Hochberg FDR with $q < 0.05$ defined as a significance cut-off.

657

658

659 **RNA Isolation**

660 Samples were harvested in trizol and frozen at -80°C until processing. RNA extraction was
661 performed first by phase separation with chloroform (200ul per 1ml of trizol) and purified using a
662 column-based procedure (Qiagen 74104) with DNase I treatment.

663

664 **RNAseq and Analysis**

665 Paired sequence reads underwent quality trimming using the Skewer (v0.2.2) with default
666 setting(Jiang et al., 2014). Subsequently, RNA-seq reads were aligned to the human reference
667 genome sequence (hg38) using STAR aligner (v2.5.3a) with default settings(Dobin et al., 2013).
668 Annotations and genome files (hg38) were obtained from Ensembl (release 105). Uniquely mapped
669 reads with a mapping quality ($Q \geq 30$) were counted across genes with featureCounts
670 (*subread* 2.0.0)(Liao et al., 2014). Using the annotation package org.Hs.eg.db, ribosomal and
671 mitochondrial genes as well as pseudogenes, and genes with no annotation (Entrez Gene ID) were
672 removed before normalization and statistical analysis. In this dataset, only genes with > 0.5 counts
673 per million (CPM) in at least 4 samples were retained for statistical analysis. Differential gene
674 expression analysis was performed in the R statistical programming language with the Bioconductor
675 packages edgeR (v3.36.0)(Robinson and Oshlack, 2010) in RStudio. A false discovery rate (FDR)
676 < 0.05 using the correction procedure of Benjamini and Hochberg(Benjamini and Hochberg, 1995)
677 was used.

678

679 **Cardiac Organoid Fabrication**

680 Human cardiac organoids (hCO) were fabricated as previously described(Mills et al., 2019; Mills et
681 al., 2017). Briefly, day 15 cardiac differentiations were dissociated to a single cell suspension. Acid

682 solubilized collagen I (Devro) was salt balanced with 10X DMEM, pH neutralized with 0.1M NaOH
683 and mixed sequentially on ice with Matrigel and cells. Each hCO contained 5×10^4 cells in 2.6mg/ml
684 collagen I and 9% Matrigel in a volume of 3.5ul. After gelling for 60 minutes at 37°C and 5% CO₂,
685 after which hCOs were cultured in α -MEM GlutaMAX (ThermoFisher Scientific), 10% FBS, 200mM
686 L-ascorbic acid 2-phosphate sesquimagnesium salt hydrate (Sigma) and 1% Penicillin/Streptomycin
687 (ThermoFisher Scientific) with media change every 2-3 days. Nine days after fabrication, active force
688 production was measured by analyzing hCO pole deflection. 10 second videos were collected at
689 100Hz using a Leica Thunder DMI8 inverted microscope. Videos were analyzed to describe
690 contractile parameters using a previously described MATLAB code(Mills *et al.*, 2017).

691

692 **Calcium Imaging**

693 Calcium imaging was performed using Fluo-4 AM (Invitrogen F-14201). Briefly, cells were incubated
694 in Tyrode's buffer (140mM NaCl, 5.4mM KCl, 1mM MgCl₂, 10mM glucose, 1.8mM CaCl₂, 10mM
695 HEPES, pH 7.4) containing 5 μ M Fluo-4AM and 0.02% pluronic acid F-127 for 30 minutes at 37°C.
696 Cells were then washed with Tyrode's buffer for 30 minutes. Line scans were collected at a frequency
697 of 100Hz using an LSM900 and 40x oil objective.

698

699 **Immunoprecipitation**

700 Lactate purified cardiomyocytes were washed with cold PBS prior to lysis in Co-IP buffer (150mM
701 NaCl, 50mM Tris-HCl, pH 7.5, 10% glycerol, 0.1% triton X-100). Lysates were incubated at 4°C with
702 agitation for 1 hour. Insoluble matter was pelleted by centrifugation at 12,000xg for 15 minutes at
703 4°C. Each reaction was incubated in 2ug of anti-FLAG M2 (Sigma F1804) for 2 hours at 4°C and
704 incubated with 40ul washed Dynabeads Protein G (Invitrogen 10003D) for 1 hour. Beads were
705 collected by magnetic separation and washed twice in cold lysis buffer followed by three washes in
706 cold PBS. Buffer was aspirated and the beads were snap frozen on dry ice.

707

708 **HEK Cell Transfection**

709 HEK-293FT cells (Invitrogen) were cultured in 1x DMEM, 10% FBS, 0.1mM non-essential amino
710 acids (ThermoFisher), 1% GlutaMAX, 1% Penicillin/streptomycin, and 500µg/ml geneticin (Gibco).
711 HEK-293FT cells were plated at 625,000 cells per well of a 6-well culture plate. Plasmids were
712 transfected using Lipofectamine 3000 (Invitrogen) in the above media without antibiotics. After 24
713 hours, media was changed refreshed to include antibiotics and cells harvested for downstream
714 applications the next day.

715

716 **Data Availability**

717 All proteomics raw data have been deposited in PRIDE: PXD035535 (total and phosphoproteomics
718 data of WT vs. *ALPK3*^{mut}) or PXD035734 (ALPK3-SBP3XFLAG affinity purification) and will be made
719 public following acceptance of the manuscript.

720

721

722

723

724

725

726

727

728 **SUPPLEMENTARY REFERENCES**

729

730 Benjamini, Y., and Hochberg, Y. (1995). Controlling the False Discovery Rate: A Practical
731 and Powerful Approach to Multiple Testing. *Journal of the Royal Statistical Society: Series*
732 *B (Methodological)* 57, 289-300. <https://doi.org/10.1111/j.2517-6161.1995.tb02031.x>.

733 Bruderer, R., Bernhardt, O.M., Gandhi, T., Miladinović, S.M., Cheng, L.Y., Messner, S.,
734 Ehrenberger, T., Zanotelli, V., Butscheid, Y., Escher, C., et al. (2015). Extending the limits
735 of quantitative proteome profiling with data-independent acquisition and application to

- 736 acetaminophen-treated three-dimensional liver microtissues. *Mol Cell Proteomics* *14*,
737 1400-1410. [10.1074/mcp.M114.044305](https://doi.org/10.1074/mcp.M114.044305).
- 738 Butler, A., Hoffman, P., Smibert, P., Papalexi, E., and Satija, R. (2018). Integrating single-
739 cell transcriptomic data across different conditions, technologies, and species. *Nature*
740 *Biotechnology* *36*, 411-420. [10.1038/nbt.4096](https://doi.org/10.1038/nbt.4096).
- 741 Dobin, A., Davis, C.A., Schlesinger, F., Drenkow, J., Zaleski, C., Jha, S., Batut, P.,
742 Chaisson, M., and Gingeras, T.R. (2013). STAR: ultrafast universal RNA-seq aligner.
743 *Bioinformatics* *29*, 15-21. [10.1093/bioinformatics/bts635](https://doi.org/10.1093/bioinformatics/bts635).
- 744 Elliott, D.A., Braam, S.R., Koutsis, K., Ng, E.S., Jenny, R., Lagerqvist, E.L., Biben, C.,
745 Hatzistavrou, T., Hirst, C.E., Yu, Q.C., et al. (2011). NKX2-5eGFP/w hESCs for isolation of
746 human cardiac progenitors and cardiomyocytes. *Nature Methods* *8*, 1037-1040.
747 [10.1038/nmeth.1740](https://doi.org/10.1038/nmeth.1740).
- 748 Humphrey, S.J., Karayel, O., James, D.E., and Mann, M. (2018). High-throughput and
749 high-sensitivity phosphoproteomics with the EasyPhos platform. *Nature Protocols* *13*,
750 1897-1916. [10.1038/s41596-018-0014-9](https://doi.org/10.1038/s41596-018-0014-9).
- 751 Jiang, H., Lei, R., Ding, S.W., and Zhu, S. (2014). Skewer: a fast and accurate adapter
752 trimmer for next-generation sequencing paired-end reads. *BMC Bioinformatics* *15*, 182.
753 [10.1186/1471-2105-15-182](https://doi.org/10.1186/1471-2105-15-182).
- 754 Liao, Y., Smyth, G.K., and Shi, W. (2014). featureCounts: an efficient general purpose
755 program for assigning sequence reads to genomic features. *Bioinformatics* *30*, 923-930.
756 [10.1093/bioinformatics/btt656](https://doi.org/10.1093/bioinformatics/btt656).

- 757 McGinnis, C.S., Murrow, L.M., and Gartner, Z.J. (2019). DoubletFinder: Doublet Detection
758 in Single-Cell RNA Sequencing Data Using Artificial Nearest Neighbors. *Cell Syst* 8, 329-
759 337.e324. [10.1016/j.cels.2019.03.003](https://doi.org/10.1016/j.cels.2019.03.003).
- 760 Mills, R.J., Parker, B.L., Quaife-Ryan, G.A., Voges, H.K., Needham, E.J., Bornot, A., Ding,
761 M., Andersson, H., Polla, M., Elliott, D.A., et al. (2019). Drug Screening in Human PSC-
762 Cardiac Organoids Identifies Pro-proliferative Compounds Acting via the Mevalonate
763 Pathway. *Cell Stem Cell* 24, 895-907.e896. <https://doi.org/10.1016/j.stem.2019.03.009>.
- 764 Mills, R.J., Titmarsh, D.M., Koenig, X., Parker, B.L., Ryall, J.G., Quaife-Ryan, G.A., Voges,
765 H.K., Hodson, M.P., Ferguson, C., Drowley, L., et al. (2017). Functional screening in
766 human cardiac organoids reveals a metabolic mechanism for cardiomyocyte cell cycle
767 arrest. *Proceedings of the National Academy of Sciences* 114, E8372-E8381.
768 [10.1073/pnas.1707316114](https://doi.org/10.1073/pnas.1707316114).
- 769 Phelan, D.G., Anderson, D.J., Howden, S.E., Wong, R.C., Hickey, P.F., Pope, K., Wilson,
770 G.R., Pébay, A., Davis, A.M., Petrou, S., et al. (2016). ALPK3-deficient cardiomyocytes
771 generated from patient-derived induced pluripotent stem cells and mutant human
772 embryonic stem cells display abnormal calcium handling and establish that ALPK3
773 deficiency underlies familial cardiomyopathy. *Eur Heart J* 37, 2586-2590.
774 [10.1093/eurheartj/ehw160](https://doi.org/10.1093/eurheartj/ehw160).
- 775 Robinson, M.D., and Oshlack, A. (2010). A scaling normalization method for differential
776 expression analysis of RNA-seq data. *Genome Biol* 11, R25. [10.1186/gb-2010-11-3-r25](https://doi.org/10.1186/gb-2010-11-3-r25).
- 777 Sim, C.B., Phipson, B., Ziemann, M., Rafehi, H., Mills, R.J., Watt, K.I., Abu-Bonsrah, K.D.,
778 Kalathur, R.K.R., Voges, H.K., Dinh, D.T., et al. (2021). Sex-Specific Control of Human

- 779 Heart Maturation by the Progesterone Receptor. *Circulation* *143*, 1614-1628.
780 [10.1161/circulationaha.120.051921](https://doi.org/10.1161/circulationaha.120.051921).
- 781 Stuart, T., Butler, A., Hoffman, P., Hafemeister, C., Papalexi, E., Mauck, W.M., 3rd, Hao,
782 Y., Stoeckius, M., Smibert, P., and Satija, R. (2019). Comprehensive Integration of Single-
783 Cell Data. *Cell* *177*, 1888-1902.e1821. [10.1016/j.cell.2019.05.031](https://doi.org/10.1016/j.cell.2019.05.031).
- 784 Stuart, T., and Satija, R. (2019). Integrative single-cell analysis. *Nat Rev Genet* *20*, 257-
785 272. [10.1038/s41576-019-0093-7](https://doi.org/10.1038/s41576-019-0093-7).
- 786 Tyanova, S., Temu, T., Sinitcyn, P., Carlson, A., Hein, M.Y., Geiger, T., Mann, M., and
787 Cox, J. (2016). The Perseus computational platform for comprehensive analysis of
788 (prote)omics data. *Nat Methods* *13*, 731-740. [10.1038/nmeth.3901](https://doi.org/10.1038/nmeth.3901).
- 789 Young, M.D., and Behjati, S. (2020). SoupX removes ambient RNA contamination from
790 droplet-based single-cell RNA sequencing data. *Gigascience* *9*.
791 [10.1093/gigascience/giaa151](https://doi.org/10.1093/gigascience/giaa151).
- 792
- 793

794 **Figure 1. ALPK3 is a myogenic kinase localized to the M-band of the sarcomere.**

795 **A.** UMAP generated from non-failing human heart snRNAseq.

796 **B.** Expression pattern of *ALPK3* within cell types of the non-failing human heart.

797 **C.** Schematic of targeting strategy of ALPK3-tdTomato hPSC cell line and flow cytometry of
798 directed cardiac differentiation.

799 **D.** Representative immunofluorescent microscopy image of nanopatterned ALPK3-
800 tdTomato hPSC-derived cardiomyocyte stained with alpha-actinin (green), obscurin (grey),
801 and tdTomato (magenta), scale bar = 5µm.

802 **E.** Schematic of targeting strategy of ALPK3-SBP3xFLAG hPSC cell line and representative
803 immunofluorescent micrograph of WT and ALPK3-SBP3xFLAG hPSC-CMs stained for
804 alpha-actinin (magenta), FLAG (green), and DAPI (blue), scale bar = 10µm.

805 **F.** Schematic of targeting strategy of ALPK3-SBP3xFLAG hPSC cell line and Western blot
806 of ALPK3 in myofilament and cytosolic fractions of cardiomyocytes.

807

808 **Figure 2. ALPK3 is required for sarcomere organization and calcium handling.**

809 **A.** *ALPK3* Gene structure, schematic of *ALPK3*^{mut} gene targeting, and graphic of cardiac
810 differentiation.

811 **B.** Representative immunofluorescent micrograph of WT and *ALPK3*^{mut} hPSC-CM's stained
812 for MYOM1 (green), alpha-actinin (purple), and DAPI (blue), scale bar = 30µm.

813 **C.** Representative line scan of Fluo-4AM calcium handling in WT and *ALPK3*^{-/-} hPSC-CMs.

814 **D.** Representative calcium transient trace of WT and *ALPK3*^{mut} hPSC-CMs.

815 **E.** Peak systolic Fluo-4AM fluorescence for WT and *ALPK3*^{mut} hPSC-CMs.

816 **F.** Percent of irregular calcium transients in WT and *ALPK3*^{mut} hPSC-CMs.

817 **G.** Time constant (tau) of diastolic calcium reuptake in WT and *ALPK3*^{mut} hPSC-CMs.
818 For calcium handling data, n=80 and 74 for WT and *ALPK3*^{mut} over 8 and 7 independent
819 replicates, respectively.

820

821 **Figure 3. ALPK3 deficiency impairs contractility in cardiac organoids.**

822 **A.** Experimental outline of human cardiac organoid (hCO) study.

823 **B.** Force traces from representative WT and *ALPK3*^{mut} hCOs.

824 **C.** Total active force production from WT and *ALPK3*^{mut} hCOs.

825 **D.** WT and *ALPK3*^{mut} hCOs beating rate per minute.

- 826 **E.** Time to 50% activation of WT and *ALPK3*^{mut} hCOs.
- 827 **F.** Time to 50% relaxation of WT and *ALPK3*^{mut} hCOs..
- 828 **G.** WT and *ALPK3*^{mut} hCOs RR scatter of hCOs to index arrhythmicity.
- 829 **H.** Immunofluorescence of WT and *ALPK3*^{mut} hCOs staining alpha-actinin (magenta) and
- 830 obscurin (green), scale bar = 10µm.
- 831 For hCO experiments, n = 87 and 50 for WT and *ALPK3*^{mut}, respectively, over 4 independent
- 832 replicates.

833

834 **Figure 4. ALPK3 deficient cardiomyocytes have compromised expression of key**

835 **cardiac protein networks.**

- 836 **A.** Experimental outline of proteomics experiment. n = 5 per group.
- 837 **B.** Volcano plot of day 14 WT and *ALPK3*^{mut} hPSC-CMs to show differential protein
- 838 expression.
- 839 **C.** Gene ontology (GO) of biological processes enriched in differentially expressed proteins
- 840 in day 14 WT and *ALPK3*^{mut} hPSC-CMs
- 841 **D.** Volcano plot of day 30 WT and *ALPK3*^{mut} hPSC-CMs to show differential protein
- 842 expression.
- 843 **E.** GO of biological processes enriched in differentially expressed proteins in day 30 WT
- 844 and *ALPK3*^{mut} hPSC-CMs.
- 845 **F.** Venn diagrams of protein expression up- or down-regulated proteins common for day 14
- 846 and day 30.
- 847 **G.** GO of biological processes of commonly up- or down-regulated proteins in *ALPK3*^{mut}
- 848 hPSC-CMs.

849

850 **Figure 5. ALPK3 is critical for phosphorylation of sarcomeric and autophagy**

851 **components.**

- 852 **A.** Experimental outline of phosphoproteomic experiments. n = 5 per group.
- 853 **B.** Volcano plot of day 14 WT and *ALPK3*^{mut} hPSC-CMs to show differential abundance of
- 854 normalized phosphopeptides.
- 855 **C.** Gene ontology (GO) terms of biological processes enriched in differentially
- 856 phosphorylated proteins between day 14 WT and *ALPK3*^{mut} hPSC-CMs.

- 857 **D.** Volcano plot of WT and *ALPK3*^{mut} hPSC-CMs to show differential abundance of
858 normalized phosphopeptides at day 30.
- 859 **E.** GO terms of biological processes enriched in differentially phosphorylated proteins
860 between day 30 WT and *ALPK3*^{mut} hPSC-CMs.
- 861 **F.** Venn diagram showing overlap of dephosphorylated phosphopeptides in *ALPK3*^{mut}
862 hPSC-CMs between day 14 and day 30.
- 863 **G.** GO terms of biological processes enriched in commonly dephosphorylated proteins in
864 *ALPK3*^{mut} hPSC-CMs between day 14 and day 30.

865

866 **Figure 6. ALPK3 binds the autophagy regulatory SQSTM1 (p62) and is required for**
867 **the sarcomeric localization of SQSTM1.**

- 868 **A.** Outline of co-immunoprecipitation experiment to identify ALPK3 interactors. Created with
869 BioRender.com.
- 870 **B.** Volcano plot of enriched peptides in ALPK3-SBP3XFLAG hPSC-CMs identified by mass
871 spectrometry. n = 5 per group.
- 872 **C.** HEK293FT co-immunoprecipitation of ALPK3-FLAG and SQSTM1-HA.
- 873 **D.** Immunofluorescent staining of ALPK3-FLAG (yellow), SQSTM1 (green), and alpha-
874 actinin (magenta) in ALPK3-SBP3XFLAG hPSC-CMs. Scale bar = 15µm.
- 875 **E.** Western blot of SQSTM1 levels in WT and *ALPK3*^{mut} hPSC-CMs.
- 876 **F.** Representative immunofluorescent staining of alpha-actinin (magenta), SQSTM1
877 (green), and DAPI (blue) in WT and *ALPK3*^{mut} hPSC-CMs. Scale bar = 15µm.
- 878 **G.** Immunofluorescent staining of MYOM1 (green) and alpha-actinin (magenta) in WT and
879 *ALPK3* patient variant hPSC-CMs. Scale bar = 15µm.
- 880 **H.** Immunofluorescent localization of SQSTM1 (green) and alpha-actinin (magenta) in WT
881 and *ALPK3* patient variant hPSC-CMs. Scale bar = 15µm.

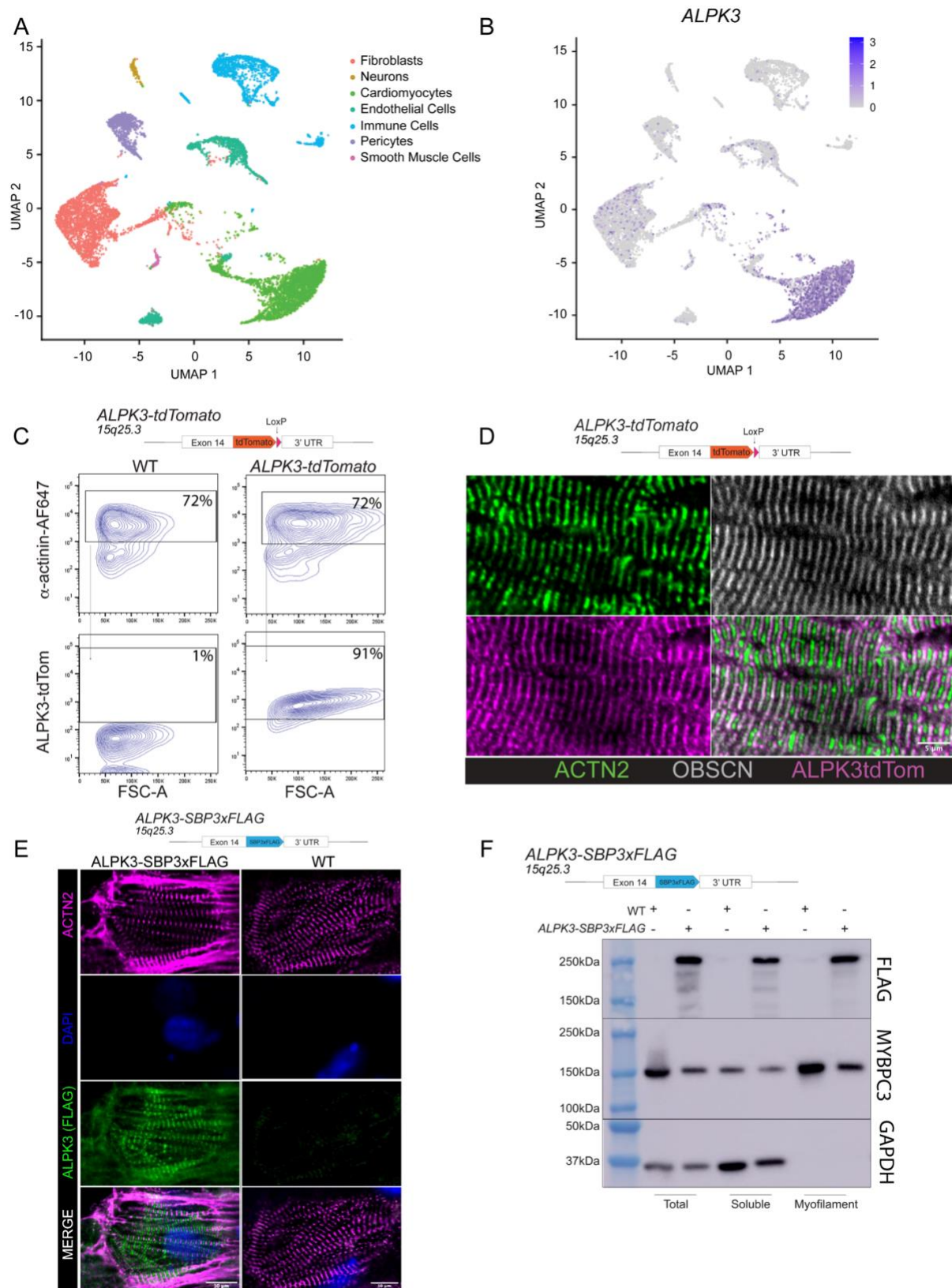
882

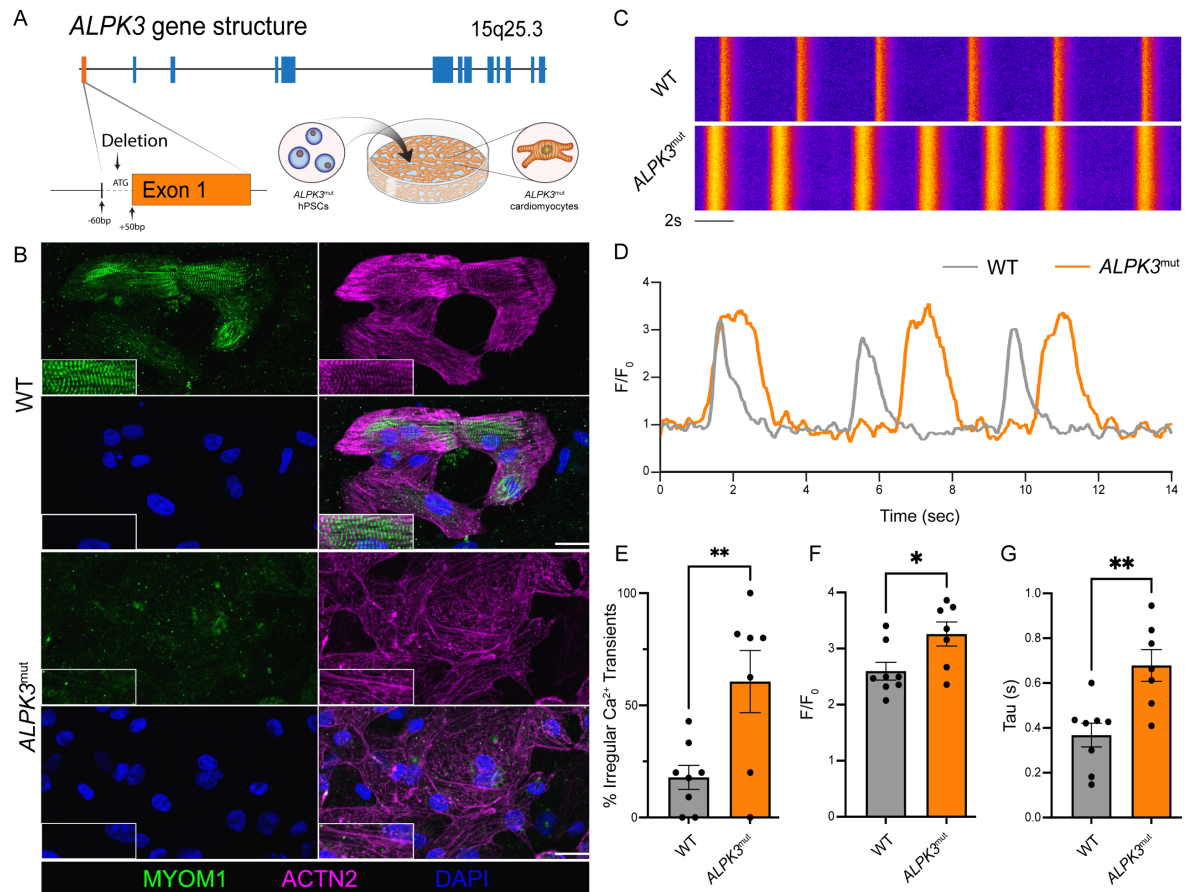
883 **Figure 7. Graphical representation of findings from this study.**

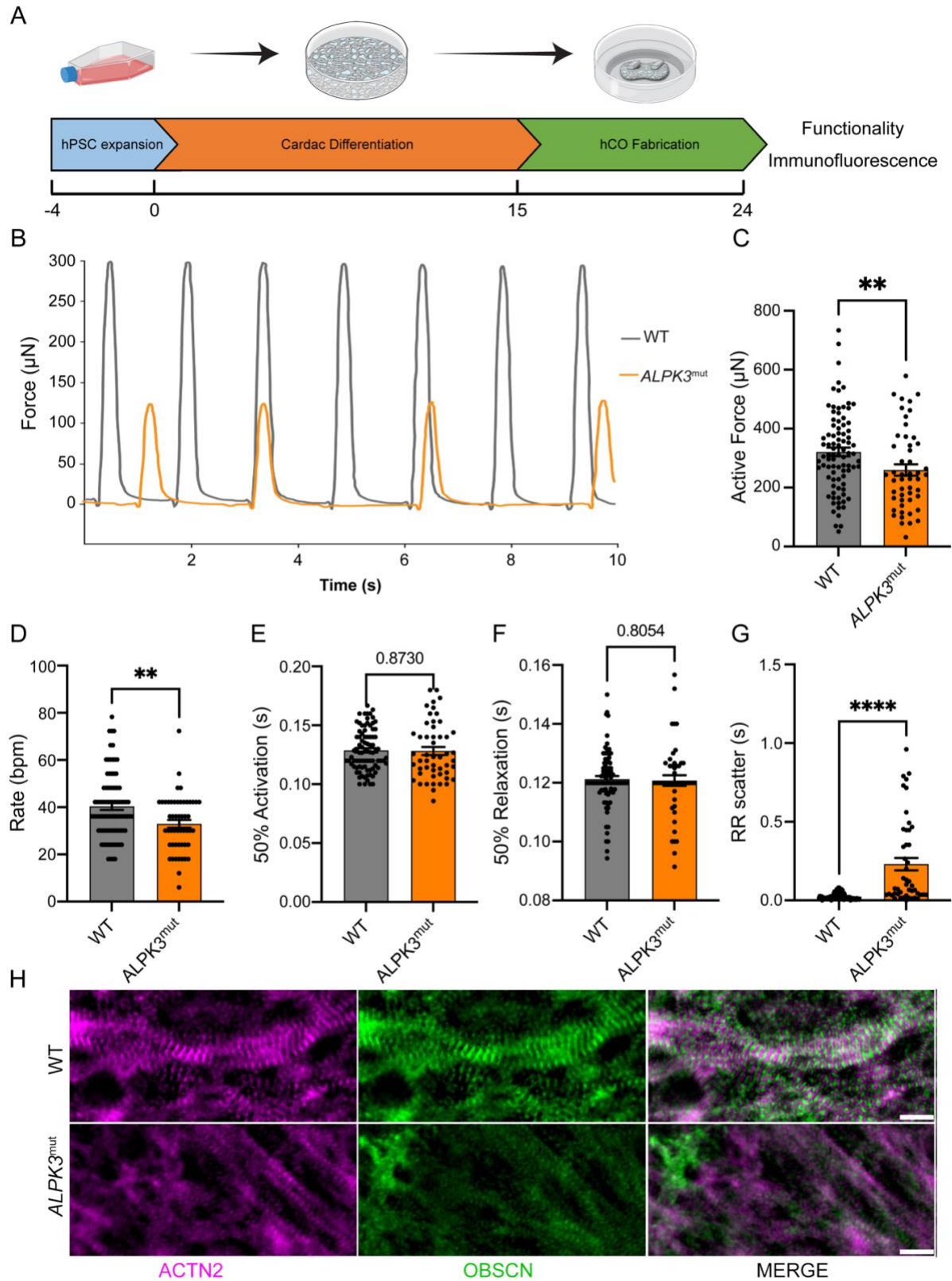
884 Graphical summary of key findings from this study of sarcomere disorganization and
885 SQSTM1 and MYOM1 mislocalization in *ALPK3*^{mut} hPSC-CMs. Created with
886 BioRender.com.

887

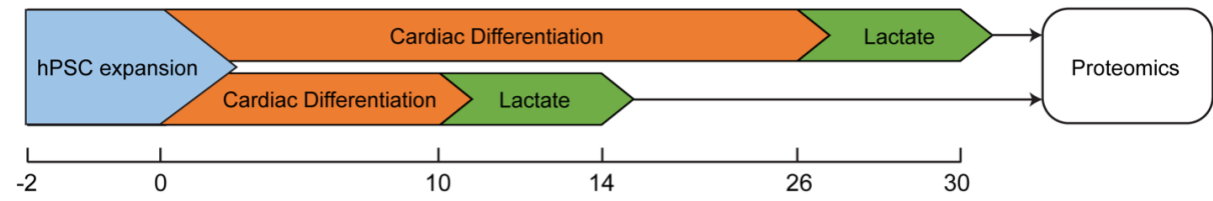
888



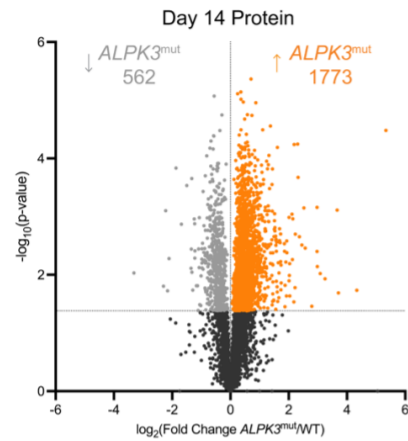




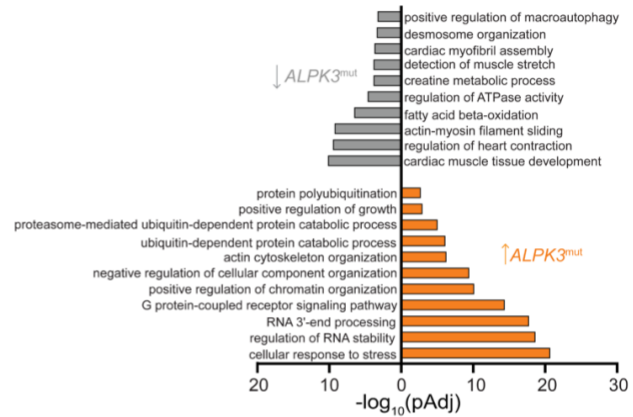
A



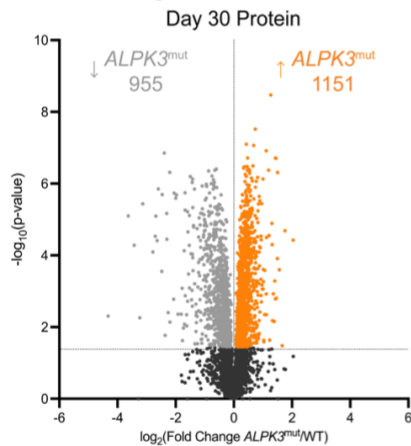
B



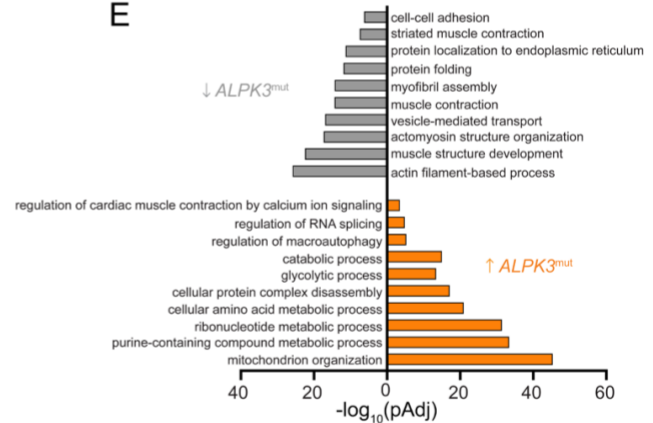
C



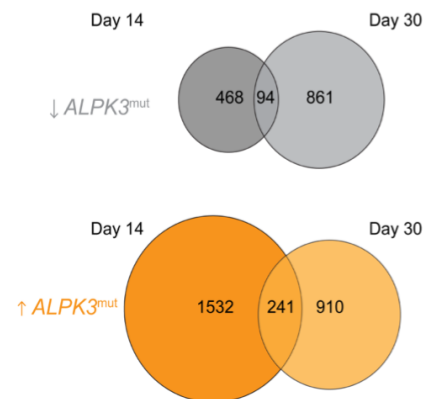
D



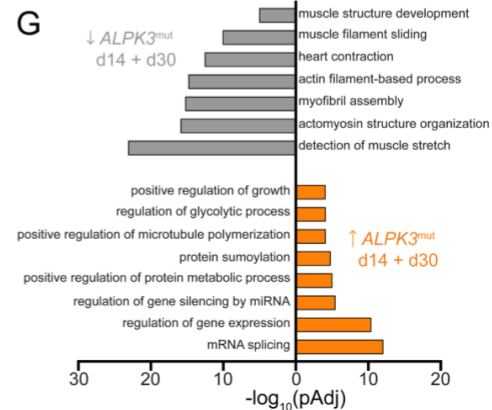
E



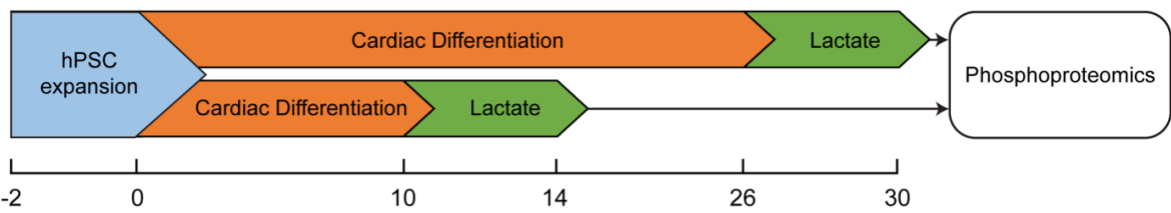
F



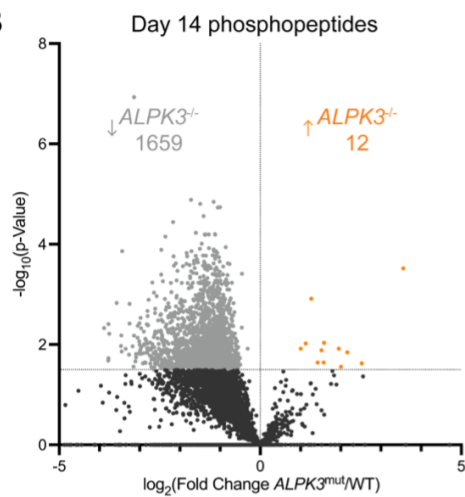
G



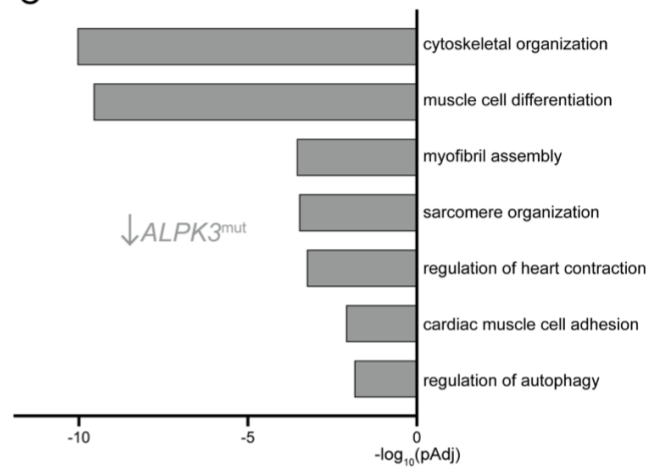
A



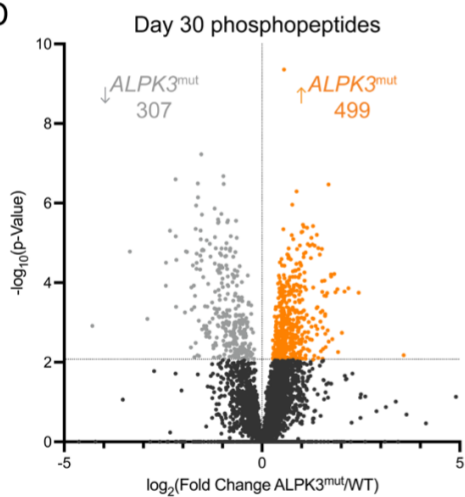
B



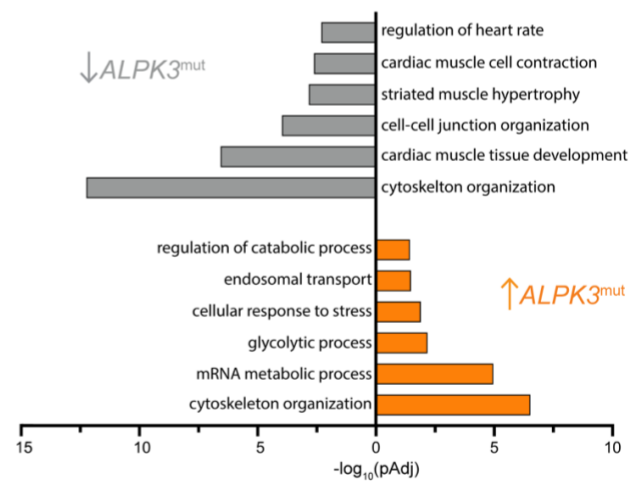
C



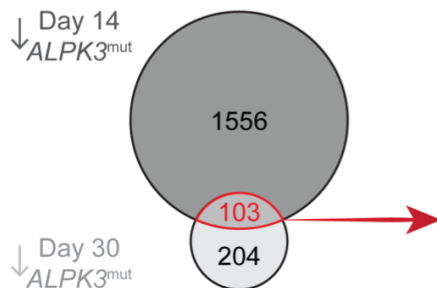
D



E



F



G

